AIP | Journal of Applied Physics

Amplifying mirrors for terahertz plasmons

O. Sydoruk, R. R. A. Syms, and L. Solymar

Citation: J. Appl. Phys. **112**, 104512 (2012); doi: 10.1063/1.4766924
View online: http://dx.doi.org/10.1063/1.4766924
View Table of Contents: http://jap.aip.org/resource/1/JAPIAU/v112/i10
Published by the American Institute of Physics.

Amplifying mirrors for terahertz plasmons

O. Sydoruk,[a] R. R. A. Syms, and L. Solymar
Optical and Semiconductor Devices Group, Department of Electrical and Electronic Engineering, Imperial College London, Exhibition Road, London SW7 2AZ, United Kingdom

(Received 29 August 2012; accepted 24 October 2012; published online 27 November 2012)

Semiconductor plasmons have long held out a promise for terahertz generation, but competitive plasmonic mechanisms have yet to be found. Here, we introduce amplifying terahertz mirrors: planar interfaces for two-dimensional electron channels that amplify plasmons in the presence of electron drift. In contrast to existing formulations, we develop a rigorous mode matching technique that takes the complete mode spectrum into account. Mirrors are characterized by plasmon reflection and transmission coefficients whose values can increase with drift. Amplitude and power coefficients are determined, and conditions are found for their values to exceed unity. Resonators based on different combinations of amplifying mirrors are investigated, and an asymmetric configuration (consisting of two different electron channels confined between conducting planes) whose roundtrip gain can exceed unity is identified. The unusual conditions needed for oscillation are examined in detail and the general advantages of asymmetric arrangements are highlighted. Finally, the potential of mode matching as a universal tool for plasmonics is discussed. © *2012 American Institute of Physics*. [http://dx.doi.org/10.1063/1.4766924]

I. INTRODUCTION

The most urgent problem of terahertz science is the need for more effective sources, and while existing methods of generation, such as photoconductive switching and photomixing,[1] are being actively refined, intensive search for alternatives is under way. Terahertz generation by semiconductor plasmons is attracting increased attention; recently studied plasmonic mechanisms include emission in grating-coupled systems,[2] plasmon-phonon interactions,[3–5] and transit-time instabilities.[6]

The current interest in plasmonic generation dates back to the pioneering study by Dyakonov and Shur of plasmons in two-dimensional channels of field-effect transistors.[7] Confined between the transistor's source and drain, the plasmons become unstable and lead to oscillations under specific boundary conditions. Dyakonov and Shur postulated them as absence of ac potential at the source and of ac conduction current at the drain and showed that the reflection coefficient at the drain exceeded unity in the presence of electron drift. Subsequent theoretical studies considered electron diffusion,[8] more general boundary conditions,[9] non-uniform channels,[9,10] etc. Other geometries, e.g., gate-less electron channels[8,11] and cylindrical transistors,[12] were also proposed.

The majority of these studies adopted the original approach of Dyakonov and Shur that essentially reduces a two-dimensional problem to a single dimension. The approach is to ignore spatial variation of the electromagnetic quantities outside the channel and to formulate boundary conditions only on the channel. Simplicity is its great advantage, often allowing problems to be solved analytically. More rigorous studies, though not concerned with instabilities, were conducted by Ryzhii, Satou, and co-authors,[13–15] who formulated boundary conditions on the whole surface of the contacts by treating them as, for example, perfectly conducting planes.[13]

Here, we present a rigorous analysis of planar plasmonic interfaces and discuss their properties in the presence of drift. The first interface is between two different two-dimensional channels, Fig. 1(a), and the second one is between a channel and a perfectly conducting plane, Fig. 1(b). As will be shown, the amplitude and power of the plasmon transmitted through or reflected from an interface can exceed that of the incident plasmon. In other words, the interfaces act as amplifying plasmonic mirrors. Resonators comprising such mirrors can have the roundtrip gain exceeding unity and may lead to terahertz oscillations.

To study the interfaces, we have developed a mode decomposition technique whose rigor and capabilities by far exceed those of the standard one-dimensional approach. The technique is described in detail in Sec. III, but the need for it can be stated already here. The dispersion curves of plasmons propagating in opposite directions are identical without but different with electron drift, see Fig. 2. The channel with drifting electrons becomes a non-reciprocal, non-bidirectional[16] waveguide. The plasmons propagating in opposite directions have different wavenumbers and, hence, decay lengths, as shown schematically in Fig. 1. Due to this difference, a plasmon incident on a perfectly conducting plane gives rise not only to a reflected plasmon but also to other, non-plasmonic, modes required to match the field at the interface. For the interface between two channels, matching the fields solely by plasmons is, naturally, impossible even in the absence of drift. Transmission and reflection of non-drifting plasmons can be studied by the mode matching techniques developed in Refs. 17–20. However, to attack the problem of drifting plasmons, we had to develop an alternative formulation.

Section II describes the configuration with a single electron channel. Section III describes transmission and reflection of plasmons by single interfaces, while Sec. IV concentrates on resonators comprising several interfaces. Section V draws conclusions.

[a]Electronic mail: osydoruk@imperial.ac.uk.

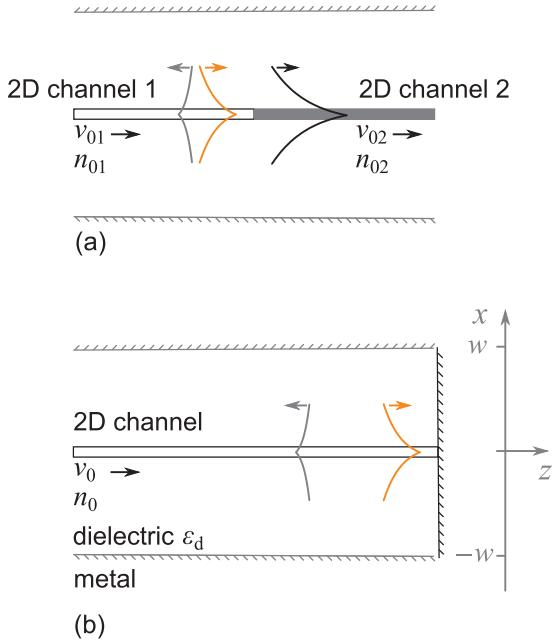

FIG. 1. Interfaces between two different electron channels (a) or between a channel and conducting plane (b) can act as amplifying mirrors for terahertz plasmons. Field matching at the interface solely by plasmons is impossible due to their different decay lengths.

II. TWO-DIMENSIONAL CHANNELS

The configuration consists of a two-dimensional channel occupying the plane $x = 0$, see Fig. 1, and having a constant electron density n_0. Electrons can drift along the z-axis with the drift velocity v_0 whose sign depends on the drift direction. The channel is sandwiched between two conducting planes placed symmetrically at a distance w from it. The main role of the planes is to prevent radiation from escaping from the interaction region. However, they can also be used as gates controlling the electron density. Dielectric with a relative permittivity ε_d surrounds the channel.

As usually done, we analyze the configuration under harmonic perturbations in two steps. First, we describe the electron dynamics by the hydrodynamic equation of motion and derive the current and electron density in the channel. We then couple them to Maxwell's equations by boundary conditions on the channel. At the heart of this approach lies a linearization procedure, carried out as follows. The total electron density in the channel is the sum of the constant (dc) and harmonically varying (ac) components, $n_0 + n\exp(\mathrm{j}\omega t)$, where $\omega = 2\pi f$ and f is the frequency. The electron velocity is, analogously, $v_0 + v\exp(\mathrm{j}\omega t)$.

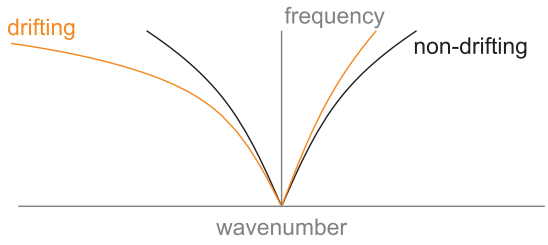

FIG. 2. Dispersion curves for non-drifting and drifting plasmons. Whereas non-drifting plasmons (black lines) have the same dispersion for opposite directions, drifting plasmons (orange lines) propagating in opposite directions have different wavenumbers.

Assuming that the amplitudes of the ac components are much smaller than their dc counterparts, we neglect all products of small ac terms. For example, the conduction current density will be equal to

$$e(n_0 + n\mathrm{e}^{\mathrm{j}\omega t})(v_0 + v\mathrm{e}^{\mathrm{j}\omega t}) \approx en_0v_0 + (en_0v + envv_0)\mathrm{e}^{\mathrm{j}\omega t},$$

where positive sign is taken for the electron charge e. Here, $J_0 = en_0v_0$ is the dc current density and

$$J = en_0v + envv_0 \tag{1}$$

is the amplitude of the linearized ac current density. Analogously, we obtain the linearized ac hydrodynamic equation of motion in the form:

$$\mathrm{j}\omega v + v_0\frac{\partial v}{\partial z} = \frac{eE_z|_{x=0}}{m}, \tag{2}$$

where E_z is the amplitude of the z-component of the electric field; m is the electron effective mass.

For interaction to occur, the electric field needs a component along the channel. Therefore, we considered TM waves with the electric field components E_x and E_z and the magnetic field component H_y. The longitudinal and transverse spatial variations of the fields have the form $\exp[-\mathrm{j}(k_xx + k_zz)]$, where k_x and k_z are wavenumbers in the x and z directions. Solution of Maxwell's equations in the dielectric demands

$$k_x^2 + k_z^2 = \varepsilon_d\omega^2/c^2, \tag{3}$$

where c is the light velocity in vacuum.

The standard boundary conditions on the channel are

$$\begin{aligned} E_z|_{x=+0} &= E_z|_{x=-0}, \\ E_x|_{x=+0} - E_x|_{x=-0} &= en/(\varepsilon_0\varepsilon_d), \\ H_y|_{x=+0} - H_y|_{x=-0} &= J. \end{aligned} \tag{4}$$

The boundary conditions on the conducting planes above and below the channel are $E_z|_{x=w} = E_z|_{x=-w} = 0$. Solution of Maxwell's equations subject to these boundary conditions yields for $x \in [0, w]$

$$\begin{aligned} H_y &= A\frac{\cos k_x(x-w)}{\cos k_xw}, \\ E_x &= A\frac{k_z}{\omega\varepsilon_0\varepsilon_d}\frac{\cos k_x(x-w)}{\cos k_xw}, \\ E_z &= -A\frac{k_x}{\mathrm{j}\omega\varepsilon_0\varepsilon_d}\frac{\sin k_x(x-w)}{\cos k_xw}, \\ J &= 2A, \\ v &= 2A\frac{\omega - k_zv_0}{en_0\omega}, \\ n &= 2A\frac{k_z}{\omega e}, \end{aligned} \tag{5}$$

where A is a constant. The waves obey a dispersion relation in the form

$$\Omega_p^2 \frac{k_x \tan k_x w}{(\omega - k_z v_0)^2} = -1, \quad (6)$$

where $\Omega_p^2 = e^2 n_0/(2m\varepsilon_0\varepsilon_d)$. Without the tangent term and for $v_0 = 0$, Eq. (6) reduces to the standard dispersion relation of a two-dimensional electron channel,[21] which has been confirmed experimentally, see, e.g., Refs. 22–24. Channels in the presence of drift have also been studied experimentally, and changes of the dispersion relation due to the Doppler term $k_z v_0$ were identified.[24,25] Deriving Eq. (6), we ignored electron collisions and diffusion which implies low-temperature operation. As has been found experimentally,[24] the presence of dc current and power dissipation does not increase the lattice temperature significantly. At high drift velocities, however, heating of electrons can occur, leading to deviations from the dispersion relation Eq. (6).[24] Fortunately, the effects considered in this paper (in contrast to, for example, the plasmon-optical phonon instability[5]) do not require high dc velocities.

Equation (6) has infinite number of generally complex solutions for k_x and k_z at a single frequency. The solutions can be separated into three groups: plasmons, waveguide modes, and evanescent waves. Plasmons have real values of k_z and imaginary values of k_x, and their field amplitudes decay exponentially away from the channel. Without drift, two plasmons propagate in opposite directions with the same transverse field distributions. In the presence of drift, up to four plasmon modes can propagate.[5,8,29] Dispersion curves of two of them are shown in Fig. 2. These plasmons will play a major role in the discussion to follow. The other two plasmons have much higher wavenumbers and are reminiscent of the slow and fast space-charge waves propagating on vacuum electron beams.[26] Although we later include these high-wavenumber plasmons in numerical calculations, they have low amplitudes and do not influence the qualitative picture of plasmon transmission and reflection. The waveguide modes have real values of both k_x and k_z and trigonometric transverse variations of the fields. The third group of evanescent waves comprises waves with complex wavenumbers.

To analyze the dispersion relation further, we defined the parameter values in Eq. (6) as follows. For the effective mass and the dielectric constant, we took values corresponding to GaAs, $m = 0.067m_0$ and $\varepsilon_d = 12.8$ at terahertz frequencies.[27] The dc electron concentration is $n_0 = 10^{11}\,\mathrm{cm}^{-2}$, the drift velocity is $v_0 = 5 \times 10^6\,\mathrm{cm/s}$ in the positive z-direction, and the dielectric thickness is 100 nm. As expected, solution of the dispersion relation for these parameters yields four plasmons, two of which are shown by circles on the horizontal axis of Re k-Im k diagram in Fig. 3. The plasmon propagating along the electron drift (positive k_z) has a smaller wavenumber than the plasmon propagating against the drift (negative k_z), consistent with Fig. 2. The dielectric is too thin to allow propagation of lossless waveguide modes. The densely packed evanescent modes shown by dots in Fig. 3 merge into continuous lines and have complex-conjugated wavenumbers for opposite directions.

If the solutions of the dispersion relation without drift, $k_z^{(0)}$, are known, the solutions for weak drift can be found by a perturbation technique as follows. Since the drift velocity is small, $|k_z^{(0)} v_0| \ll \omega$, we can expand k_z in the presence of drift in a Taylor series and retain only the first two terms, so that

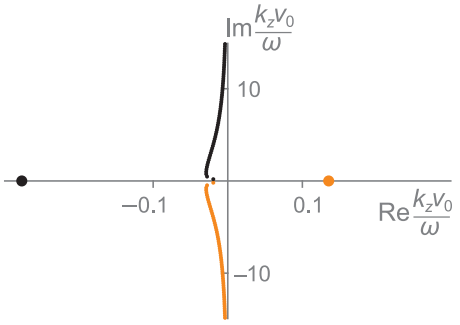

FIG. 3. Mode spectrum of a two-dimensional channel at a single frequency (1 THz). The system supports two plasmons propagating in opposite directions with different propagation constants (circles on the horizontal axis) and infinite number of evanescent modes with complex propagation constants (dots merging into continuous lines). There are no waveguide modes due to the small dielectric thickness ($w = 100$ nm).

$$k_z = k_z^{(0)} + \delta k_z, \quad (7)$$

where $|\delta k_z| \ll |k_z^{(0)}|$. Substituting Eq. (7) into Eqs. (3) and (6) and ignoring the higher-order terms in the series expansions, yields

$$\delta k_z = -\frac{2k_x^{(0)2}\omega}{k_x^{(0)2}\Omega_p^2 w + \omega^2\left(\frac{\omega^2 w}{\Omega_p^2} - 1\right)} v_0 . \quad (8)$$

In Sec. III B, we use Eq. (8) to obtain an analytical expression for the reflection coefficient of a plasmon incident on a conducting plane.

According to the ac kinetic power theorem,[26,28] the total ac power carried by a mode can be written as

$$P = \mathrm{Re}\int_0^w E_x H_y^* \mathrm{d}x + \frac{mv_0}{2e}\mathrm{Re}(vJ^*), \quad (9)$$

where asterisk denotes complex conjugation. The first term in the equation denotes electromagnetic power due to the fields, and the second one, kinetic power due to the movement of electrons. As substituting Eq. (5) into Eq. (9) shows any evanescent mode with complex wavenumber k_z carries electromagnetic and kinetic power of equal magnitude in opposite directions. Thus, its total power is zero. On the other hand, plasmons, having real wavenumbers, are able to carry power. Their kinetic power flows in the direction of drift, whereas the direction of the electromagnetic power flow coincides with the propagation direction. Power relations for plasmons are discussed in detail in Sec. III.

III. AMPLIFYING MIRRORS

This section discusses transmission and reflection of drifting plasmons by the planar interfaces of Fig. 1. As already stated in Sec. I, a single plasmon incident on an interface will, in general, excite an infinite number of reflected and transmitted waves. The fields, electron density, velocity,

and current on both sides of the interface can be presented as superposition of individual waves. Their amplitudes are then determined from the interface boundary conditions. We approach the mode decomposition problem separately for the two interfaces.

A. Interface between two electron channels

The first interface, see Fig. 1(a), is between two channels with different dc electron densities, denoted as $n_0^{(1)}$ and $n_0^{(2)}$, but equal electron masses. The interface is abrupt with the density jump at $z=0$. In the presence of drift, the dc current density is conserved, so that

$$n_0^{(1)} v_0^{(1)} = n_0^{(2)} v_0^{(2)}, \tag{10}$$

thus, determining the ratio of the drift velocities $v_0^{(1)}$ and $v_0^{(2)}$. The same dielectric surrounds both channels.

If a plasmon is incident from the left channel, the electric field component to the left of the interface is

$$E_x^{(1)}(x)|_{z=0} = E_{x1}^{(1)+} + \sum_\alpha R_\alpha E_{x\alpha}^{(1)-}. \tag{11}$$

Here the superscripts $^+$ and $^-$ denote the propagation direction. The numerical subscript α denotes the mode number. Plasmons have $\alpha = 1$, and the rest of the modes are sorted by increasing $|\mathrm{Im}\, k_z|$. The summation runs from 1 to ∞. The amplitude of the incident plasmon is taken as 1, and R_α are the mode reflection coefficients.

The right channel will propagate transmitted waves, so that

$$E_x^{(2)}(x)|_{z=0} = \sum_\alpha T_\alpha E_{x\alpha}^{(2)+}, \tag{12}$$

where T_α are the mode transmission coefficients. Expressions analogous to Eqs. (11) and (12) can be written for all other ac quantities. Relations between the ac quantities at the interface are given by the boundary conditions. Outside the channel, the interface is a continuous dielectric, and the standard dielectric boundary conditions apply

$$\begin{aligned} E_x^{(1)}(x)|_{z=0} &= E_x^{(2)}(x)|_{z=0}, \\ H_y^{(1)}(x)|_{z=0} &= H_y^{(2)}(x)|_{z=0}. \end{aligned} \tag{13}$$

Substituting Eq. (13) into the second and third equations of Eq. (4), the boundary conditions for the current and the electron densities at the interface can be determined as[29]

$$\begin{aligned} n^{(1)}|_{z=0} &= n^{(2)}|_{z=0}, \\ J^{(1)}|_{z=0} &= J^{(2)}|_{z=0}. \end{aligned} \tag{14}$$

The boundary conditions for the ac velocity can be found by substituting Eqs. (13) and (14) into Eq. (1) as

$$v^{(1,2)}|_{z=0} = \frac{2}{en_0^{(1,2)}} H_y^{(2,1)}\Big|_{\substack{x=0\\z=0}} - \frac{2\varepsilon_0\varepsilon_d v_0^{(1,2)}}{en_0^{(1,2)}} E_x^{(2,1)}\Big|_{\substack{x=0\\z=0}}. \tag{15}$$

Substituting Eqs. (11) and (12) and their equivalents for the other ac quantities into the boundary conditions yields at $z=0$

$$\begin{aligned} H_{y1}^{(1)+} + \sum_\alpha R_\alpha H_{y\alpha}^{(1)-} &= \sum_\alpha T_\alpha H_{y\alpha}^{(2)+}, \\ E_{x1}^{(1)+} + \sum_\alpha R_\alpha E_{x\alpha}^{(1)-} &= \sum_\alpha T_\alpha E_{x\alpha}^{(2)+}, \\ J_1^{(1)+} + \sum_\alpha R_\alpha J_\alpha^{(1)-} &= \sum_\alpha T_\alpha J_\alpha^{(2)+}, \end{aligned} \tag{16}$$

together with

$$\begin{aligned} v_1^{(1)+} + \sum_\alpha R_\alpha v_\alpha^{(1)-} = \frac{2}{en_0^{(1)}} \sum_\alpha T_\alpha H_{y\alpha}^{(2)+}|_{x=0} \\ - \frac{2\varepsilon_0\varepsilon_d v_0^{(1)}}{en_0^{(1)}} \sum_\alpha T_\alpha E_{x\alpha}^{(2)+}|_{x=0} \end{aligned} \tag{17}$$

and

$$\begin{aligned} \frac{2}{en_0^{(2)}} \left(H_{y1}^{(1)+}|_{x=0} + \sum_\alpha R_\alpha H_{y\alpha}^{(1)-}|_{x=0} \right) - \frac{2\varepsilon_0\varepsilon_d v_0^{(2)}}{en_0^{(2)}} \\ \times \left(E_{x1}^{(1)+}|_{x=0} + \sum_\alpha R_\alpha E_{x\alpha}^{(1)-}|_{x=0} \right) = \sum_\alpha T_\alpha v_\alpha^{(2)+}. \end{aligned} \tag{18}$$

The standard approach to solving mode equations is to rely on mode orthogonality. One has to be careful, however, when adopting the formulations developed for dielectric and metallic waveguides. Even for passive plasmonic waveguides, the mode-orthogonality conditions may differ from those in dielectric waveguides.[30] Here, the situation is further complicated by the presence of drift. Fortunately, the problem of mode orthogonality, like that of mode power, was considered in the theory of electron beams some time ago.[31] The unconjugated form of the orthogonality condition can be written as

$$\begin{aligned} \int_0^w \left(E_{x\alpha}^{(1,2)} H_{y\beta}^{(1,2)} + E_{x\beta}^{(1,2)} H_{y\alpha}^{(1,2)} \right) \mathrm{d}x + \frac{m v_0^{(1,2)}}{2e} \\ \times \left(J_\alpha^{(1,2)} v_\beta^{(1,2)} + J_\beta^{(1,2)} v_\alpha^{(1,2)} \right) = 0, \end{aligned} \tag{19}$$

for $\alpha \neq \beta$. If $v_0 = 0$, Eq. (19) reduces to the standard orthogonality condition for the fields.[32] Its conjugated form also holds and is related to the expression for mode power Eq. (9).

The present problem further distinguishes itself by the choice of the basis functions. In a reciprocal waveguide, for every mode with wavenumbers (k_z, k_x), there is a mode propagating in the opposite direction with the same transverse variation, $(-k_z, k_x)$. As a result, two identical bases are constructed from the modes propagating in opposite directions. In our non-reciprocal, non-bidirectional waveguide, modes propagating in opposite directions are mutually orthogonal, and are, therefore, able to form two different bases. Having tested both, we obtained the best numerical accuracy when using the basis of modes propagating in positive z-direction for the left waveguide and of modes propagating in the negative z-direction for the right one.

Numerically, we formulated the problem as follows. We multiplied the first two of Eqs. (16) by $E_{x\beta}^{(2)-}$ and $H_{y\beta}^{(2)-}$ ($\beta = 1, 2, \ldots$ is a mode number), respectively, added, and integrated them over the transverse coordinate. To the result, we added the third of Eqs. (16) and (18) multiplied by $mv_0^{(2)}v_\beta^{(2)-}/(2e)$ and $mv_0^{(2)}J_\beta^{(2)-}/(2e)$, respectively. Due to mode orthogonality in the right waveguide, we were then able to eliminate all terms containing transmitted modes, resulting in infinite number of equations of the form:

$$F_\beta^{(1)+} + \sum_{\alpha=1}^{\infty} R_\alpha F_{\alpha\beta}^{(1)} = 0, \tag{20}$$

where, using Eq. (5)

$$\begin{aligned} F_{\alpha\beta}^{(1)} &= 2\int_0^w \left(H_{y\alpha}^{(1)-}E_{x\beta}^{(2)-} + E_{x\alpha}^{(1)-}H_{y\beta}^{(2)-}\right)\mathrm{d}x + \frac{mv_0^{(2)}}{e}\left[J_\alpha^{(1)-}v_\beta^{(2)-} + \frac{2\varepsilon_0\varepsilon_\mathrm{d}v_0^{(2)}}{en_0^{(2)}}J_\beta^{(2)-}\left(\frac{H_{y\alpha}^{(1)-}|_{x=0}}{\varepsilon_0\varepsilon_\mathrm{d}v_0^{(2)}} - E_{x\alpha}^{(1)-}|_{x=0}\right)\right] \\ &= \frac{2}{\omega\varepsilon_\mathrm{d}\varepsilon_0}\frac{1}{k_{z\alpha}^{(1)+} - k_{z\beta}^{(2)-}}\left[\left(\frac{\omega - k_{z\alpha}^{(1)+}v_0^{(1)}}{\Omega_\mathrm{p}^{(1)}}\right)^2 - \left(\frac{\omega - k_{z\beta}^{(2)-}v_0^{(2)}}{\Omega_\mathrm{p}^{(2)}}\right)^2\right] + \frac{2v_0^{(2)}}{\varepsilon_0\varepsilon_\mathrm{d}\omega{\Omega_\mathrm{p}^{(2)}}^2}\left[2\omega - \left(k_{z\alpha}^{(1)+} + k_{z\beta}^{(2)-}\right)v_0^{(2)}\right]. \end{aligned} \tag{21}$$

To obtain $F_\beta^{(1)+}$, we set $\alpha = 1$ and replaced the superscript $^{(1)-}$ with $^{(1)+}$ in Eq. (21).

Repeating the above calculation for the basis set $(H_{y\beta}^{(1)+}, E_{x\beta}^{(1)+}, J_\beta^{(1)+}, v_\beta^{(1)+})$ and using mode orthogonality in the left waveguide, we were able to eliminate all reflected modes, so that

$$N_1^{(1)+}\delta_{1\beta} = \sum_{\alpha=1}^{\infty} T_\alpha F_{\alpha\beta}^{(2)}, \tag{22}$$

where

$$\begin{aligned} N_1^{(1)+} &= 4\int_0^w E_{x1}^{(1)+}H_{y1}^{(1)+}\mathrm{d}x + \frac{2mv_0^{(1)}}{e}J_1^{(1)+}v_1^{(1)+} \\ &= \frac{4k_{z1}^{(1)+}}{\varepsilon_0\varepsilon_\mathrm{d}\omega\cos^2\left(k_{x1}^{(1)+}w\right)}\left[\frac{w}{2} + \frac{\sin\left(2k_{x1}^{(1)+}w\right)}{4k_{x1}^{(1)+}w}\right] \\ &\quad + \frac{4v_0^{(1)}}{\varepsilon_0\varepsilon_\mathrm{d}\omega{\Omega_\mathrm{p}^{(1)}}^2}\left(\omega - k_{z1}^{(1)+}v_0^{(1)}\right), \end{aligned} \tag{23}$$

$\delta_{1\beta}$ is Kronecker's delta; and $F_{\alpha\beta}^{(2)}$ can be obtained from Eq. (21) by changing $k_{z\alpha}^{(1)+}$ to $k_{z\beta}^{(1)+}$, $k_{z\beta}^{(2)-}$ to $k_{z\alpha}^{(2)+}$ and interchanging $\Omega_\mathrm{p}^{(1)}$ with $\Omega_\mathrm{p}^{(2)}$ and $v_0^{(1)}$ with $v_0^{(2)}$. Limiting the number of modes, we truncated the sums in Eqs. (20) and (22), resulting in two independent matrix equations that can be solved numerically.

Appropriate parameters are needed for numerical models. Our main interest is in the effect of the electron drift, and we varied therefore the electron drift velocity in a wide range. For the remaining parameters, we set the value of frequency at 1 THz and chose the dc electron density in the channels as $n_0^{(1)} = 10^{11}\,\mathrm{cm}^{-2}$ and $n_0^{(2)} = 10^{12}\,\mathrm{cm}^{-2}$. The dielectric thickness was $w = 100\,\mathrm{nm}$, and the dielectric constant was $\varepsilon_\mathrm{d} = 12.8$, as used in Fig. 3. We estimated the numerical accuracy by observing conservation of electromagnetic power (see discussion below). For several hundred modes, the relative error of electromagnetic power conservation was of the order of 10^{-4}.

First, we considered plasmon incident in the left waveguide (with $n_0^{(1)} = 10^{11}\,\mathrm{cm}^{-2}$). For weak drift, the variation of the plasmon reflection and transmission coefficients is slow and approximately linear with drift velocity, see Fig. 4(a). The absolute values of both coefficients increase if the drift velocity is positive (coincides with the incidence direction) and decrease if the drift velocity is negative. The variation remains slow at high positive drift velocities (the maximum dc current density of 0.1 A/cm corresponds to the dc drift velocity in the left waveguide of about $6 \times 10^6\,\mathrm{cm/s}$), but both $|R|$ and $|T|$ decrease rapidly when the drift velocity is negative.

The coefficients R and T characterise the amplitudes but not the powers of the reflected and transmitted plasmons. The power reflection and transmission coefficients are given by $R_\mathrm{p} = P^{(1)-}/P^{(1)+}$ and $T_\mathrm{p} = P^{(2)+}/P^{(1)+}$, where the incident, $P^{(1)+}$, reflected, $P^{(1)-}$, and transmitted, $P^{(2)+}$, powers are given by Eq. (9). At zero drift velocities, the absolute values of power reflection and transmission coefficients are 0.49 and 0.51, respectively, see Fig. 4(b). As expected, the sum of the transmitted and reflected powers is equal to the incident power. In the presence of drift, this relationship breaks down.

For negative drift velocities, the interface amplifies the plasmon power. The powers of both the incident and reflected plasmons increase, and their sum exceeds that of the incident power, see Figs. 4(b) and 4(c). Moreover, the reflected power alone can exceed the incident power if the drift velocity is sufficiently large, see Fig. 4(b). For positive drift velocities, the situation reverses, and the interface absorbs power. The transmitted and reflected plasmons carry less power than in the absence of drift, and their sum is smaller than the power of the incident plasmon.

The total power carried by a plasmon is the sum of its electromagnetic and kinetic powers, see Eq. (9). These powers transform differently at the interface. The electromagnetic power is determined by the fields E_x and H_y. Since these are continuous at the interface, the electromagnetic

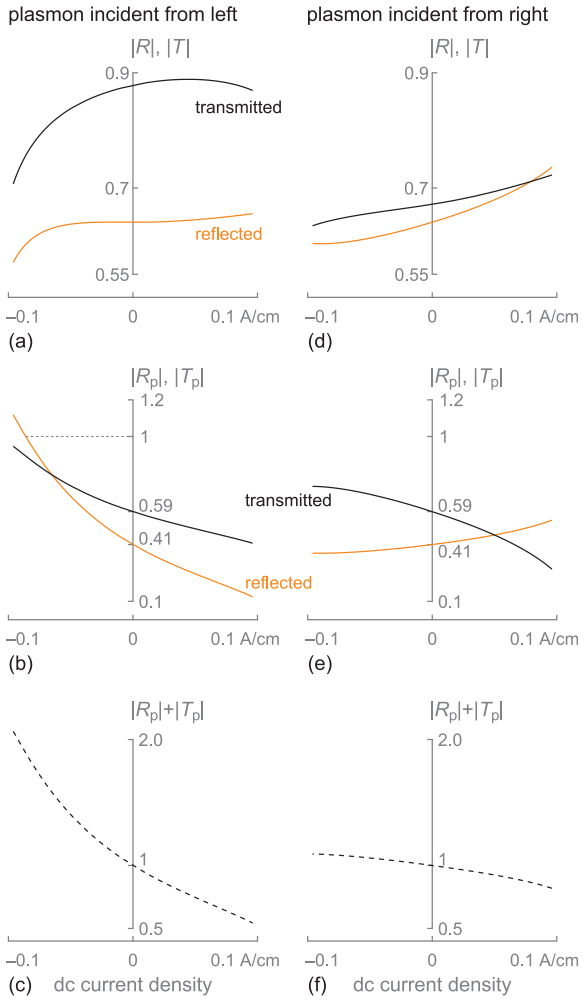

FIG. 4. Amplitude and power reflection and transmission coefficients of plasmons against the dc current density. The plasmons can be amplified: the amplitude (a) and (d), and the power (b) and (e), coefficients can exceed those in the absence of drift, and the combined power of the reflected and transmitted plasmons (c) and (f), can exceed that of the incident plasmon. Plasmons are incident from the left in (a)–(c) and from the right in (d)–(f).

powers are equal in both waveguides. It is, therefore, the jump in the kinetic power that causes the total power to be amplified or absorbed at the interface. From Eq. (9), the kinetic power is $(mv_0/2e)\mathrm{Re}(vJ^*)$, and since the current density J is continuous at the interface, the change of the kinetic power is due to the change of the dc and ac electron velocities.

Next, we considered plasmon incident in the right waveguide (with $n_0^{(2)} = 10^{12}\,\mathrm{cm}^{-2}$). The absolute values of the amplitude reflection and transmission coefficients increase with positive and decrease with negative drift velocities, see Fig. 4(d). Without drift, $|R|$ is equal to that of the plasmon incident from the opposite direction. The power of the transmitted plasmon grows with negative and decays with positive drift velocities, while the power of the reflected plasmon does the opposite, see Fig. 4(e). Their sum is equal to unity without drift, larger than unity for negative drift velocities and smaller than unity for positive drift velocities, see Fig. 4(f).

Thus, the power of the plasmon incident on the interface from either direction is amplified when the drift velocity points from the channel with higher to the channel with lower dc electron density. The effect is stronger for higher drift velocities and when the plasmon is incident in the channel with lower electron density. The power of the transmitted or reflected plasmon is larger with drift than without it if the propagation direction coincides with the drift direction.

The only non-attenuating waves in our configuration, plasmons determine the distributions of ac quantities far from the interface. When the plasmon is incident from the left, only the transmitted plasmon is present in the right waveguide away from the interface. The absolute values of, for example, E_x and H_y field components are constant in the z-direction and decay in the x-direction, as shown in Fig. 5 for $J_0 = 0.05\,\mathrm{A/cm}$. The field distributions in the left waveguide are given by superposition of the incident and reflected plasmons. In the vicinity of the interface, on the other hand, evanescent modes play a role. As shown in Fig. 5, these modes extend to about 100 nm in the left waveguide and 200 nm in the right one distorting the field distributions.

B. Interface between an electron channel and a conducting plane

The second interface is between a two-dimensional channel and a perfectly conducting plane, see Fig. 1(b). The standard interface boundary condition is the absence of the tangential component of the electric field

$$E_x|_{z=0} = 0. \tag{24}$$

Due to different decay lengths of the incident and reflected drifting plasmons, evanescent modes will be excited at the

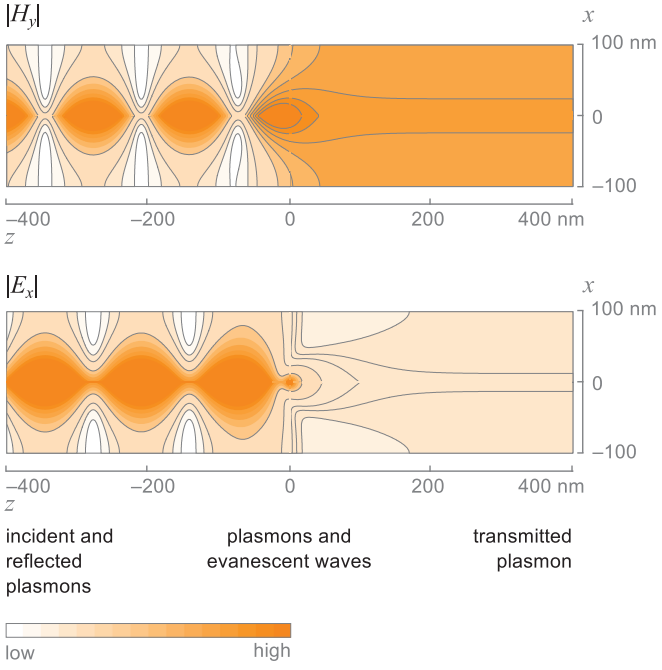

FIG. 5. Distributions of electric and magnetic fields established when a drifting plasmon is incident from the left on a two-channel interface, placed at $z = 0$. Far from the interface, the distributions show interference between the incident and reflected plasmons and the reflected plasmon. Close to the interface, up to about 100–200 nm, evanescent waves distort the field patterns.

interface to satisfy the boundary condition, so that the above equation takes the form:

$$E_{x1}^{+}|_{z=0} + \sum_{\alpha} R_{\alpha} E_{x\alpha}^{-}|_{z=0} = 0. \tag{25}$$

This is the only electrodynamic boundary condition given for a conducting plane, and the relationships between the other ac quantities, constituting the orthogonality condition Eq. (19), are not known in advance. As a result, our approach to solving Eq. (25) numerically differed from that of Sec. III A as follows. Multiplying Eq. (25) by $E_{x\beta}^{-}|_{z=0}$ and integrating the result over the transverse coordinate x, we obtained an infinite system of equations in the form:

$$F_{1\beta}^{+} + \sum_{\alpha} R_{\alpha} F_{\alpha\beta}^{-} = 0, \tag{26}$$

where

$$F_{1\beta}^{+} = -\frac{v_0}{w\Omega_p^2} \frac{2\omega - (k_{z1}^{+} + k_{z\beta}^{-})v_0}{k_{z1}^{+} + k_{z\beta}^{-}}, \tag{27}$$

$$F_{\alpha\beta}^{-} = -\frac{k_{z\beta}^{-}}{k_{z1}^{+}} \frac{v_0}{w\Omega_p^2} \frac{2\omega - (k_{z\alpha}^{-} + k_{z\beta}^{-})v_0}{k_{z\alpha}^{-} + k_{z\beta}^{-}}, \tag{28}$$

for $\alpha \neq \beta$ and

$$F_{\alpha\alpha}^{-} = \frac{k_{z\alpha}^{-}}{k_{z1}^{+}} \frac{1}{\cos(k_{x\alpha}^{-} w)} \left[\frac{w}{2} + \frac{\sin(2k_{x\alpha}^{-} w)}{4k_{x\alpha}^{-}}\right]. \tag{29}$$

Limiting the number of modes, we reduced Eq. (26) to a matrix equation that can be solved numerically for R_α.

In addition to the numerical solution of Eq. (25), we obtained an approximate analytical one as follows. Assuming weak drift and using a perturbation technique, we have already obtained an analytical approximation for the wave numbers, Eqs. (7) and (8). The same argument can be applied to the fields, so that

$$E_{x\alpha}^{\pm} = E_{x\alpha}^{(0)\pm} + \delta E_{\alpha}^{\pm}, \quad |\delta E_{\alpha}^{\pm}| \ll |E_{x\alpha}^{(0)\pm}|, \tag{30}$$

where $E_{x\alpha}^{(0)}$ is the field in the absence of drift. In addition, we can write for the reflection coefficients

$$R_{\alpha} = R_{\alpha}^{(0)} + \delta R_{\alpha}, \quad |\delta R_{\alpha}| \ll |R_{\alpha}^{(0)}|. \tag{31}$$

The values of the reflection coefficients without drift are $R_1^{(0)} = 1$ and $R_{\alpha}^{(0)} = 0$, $\alpha \neq 1$.

Substituting Eqs. (30) and (31) into the boundary condition Eq. (25) and ignoring products of small terms $\delta R_\alpha \times \delta E_\alpha^-$, we get

$$\sum_{\alpha} \delta R_{\alpha} E_{x\alpha}^{(0)+} = \delta E_{x1}^{+} + \delta E_{x1}^{-}. \tag{32}$$

Due to mode orthogonality in the absence of drift

$$\int_0^w E_{x\alpha}^{(0)+} E_{x\beta}^{(0)+} \mathrm{d}x = 0, \quad \alpha \neq \beta, \tag{33}$$

so that Eq. (32) yields

$$\delta R_{\alpha} = \frac{\int_0^w (\delta E_{x1}^{+} + \delta E_{x1}^{-}) E_{x\alpha}^{(0)+} \mathrm{d}x}{\int_0^w \left(E_{x\alpha}^{(0)+}\right)^2 \mathrm{d}x}. \tag{34}$$

Expanding the expression for E_x, see Eq. (5), we get $\delta E_{x1}^{+} = \delta E_{x1}^{-}$ and

$$\delta E_{x1}^{+} = \delta k_z^{(0)} E_{x1}^{(0)+} \left[-\frac{k_{x1}^{(0)}}{k_{z1}^{(0)^2}} + w \tan\left(k_{x1}^{(0)} w\right) - (x - w)\tan\left(k_{x1}^{(0)}(x - w)\right)\right]. \tag{35}$$

Using Eq. (35), the integrals in Eq. (34) can be found analytically. For calculations, we chose the same parameter values as in Sec. III A.

Similar to the two-channel interfaces, the conducting plane can act as an amplifying mirror. The absolute value of the plasmon reflection coefficient, $|R|$, exceeds unity for negative drift velocities (drift away from the plane), see Figs. 6(a) and 6(c). For positive drift velocities, $|R| < 1$. The effects are stronger for the smaller dc electron density of 10^{11} cm^{-2}, see Fig. 6(a). The analytical and numerical results agree for weak drift in Fig. 6(a) and coincide for the whole range in Fig. 6(c). The powers of the reflected plasmons follow the same trend, see Figs. 6(b) and 6(d): they are amplified upon reflection if the incident plasmons propagate against the drift.

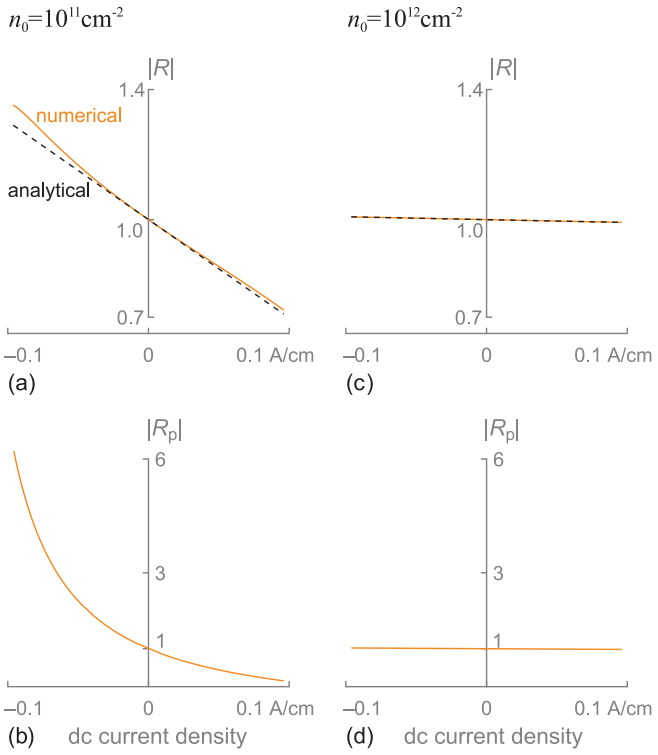

FIG. 6. Amplitude and power reflection coefficients of plasmons incident on a conducting plane exceed unity when the drift is directed away from the plane. Amplification is larger for small dc electron density (a) and (b).

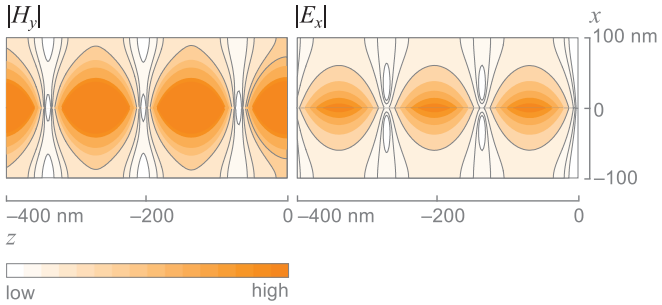

FIG. 7. Distributions of electric and magnetic fields established when a drifting plasmon is incident on a conducting-plane interface, placed at $z = 0$. The incident and reflected plasmons form the field patterns away from the interface, while close to it, the evanescent waves play additional role, compare with Fig. 5.

Far from the interface, the spatial distributions of the ac quantities are given by interference of the incident and reflected plasmon, see Fig. 7 showing the distributions of $|H_y|$ and $|E_x|$ for $n_0 = 10^{11}\,\mathrm{cm}^{-2}$ and $J_0 = 0.05\,\mathrm{A/cm}$. Close to the plane, evanescent waves distort the field distributions, as they did for the two-channel interfaces (compare with Fig. 5).

IV. RESONATORS AND OSCILLATORS

Since individual mirrors amplify plasmons, resonators made of them could lead to plasmonic generation. This section discusses two- and three-mirror Fabry-Perot resonators. Their properties will be determined solely by plasmons if the evanescent waves excited at one end of the resonator do not reach the opposite end. Hence, we assumed that the resonators were longer than 200 nm, the distance up to which the evanescent waves extended in our numerical examples, see Figs. 5 and 7.

Three different two-mirror resonators can be made of the mirrors considered in Sec. III: a channel confined between two conducting planes, Fig. 8(a), a channel confined between two channels with a different dc electron density, Fig. 8(c), and a channel confined between a conducting plane on one side and another channel on the other, Fig. 8(e). The quantity of most interest to us is the resonator roundtrip gain, G, equal to the product of the reflection coefficients of the plasmons propagating inside the resonator; oscillations occur if $|G| > 1$.

For the resonator formed by the two conducting planes, Fig. 8(a), drift has no effect on the roundtrip gain at low drift velocities, see Fig. 8(b), even though the reflection coefficients of the individual mirrors change with drift. It happens because the drift direction is opposite for the two mirrors. Electrons flow towards the right mirror, as in Fig. 8(a), and the reflection coefficient decreases from unity, see Figs. 6(a) and 6(c). On the other hand, electrons flow away from the left mirror making the reflection coefficient increase. The increase and decrease of the reflection coefficients compensate each other, as could also be anticipated from Eqs. (31) and (34). At high drift velocities, the roundtrip gain drops by 2.5% due to excitation of the high-wavenumber plasmons.

The behavior of the resonators of the second type, Fig. 8(c), depends on the relationship between the dc electron densities. When a channel with higher electron density

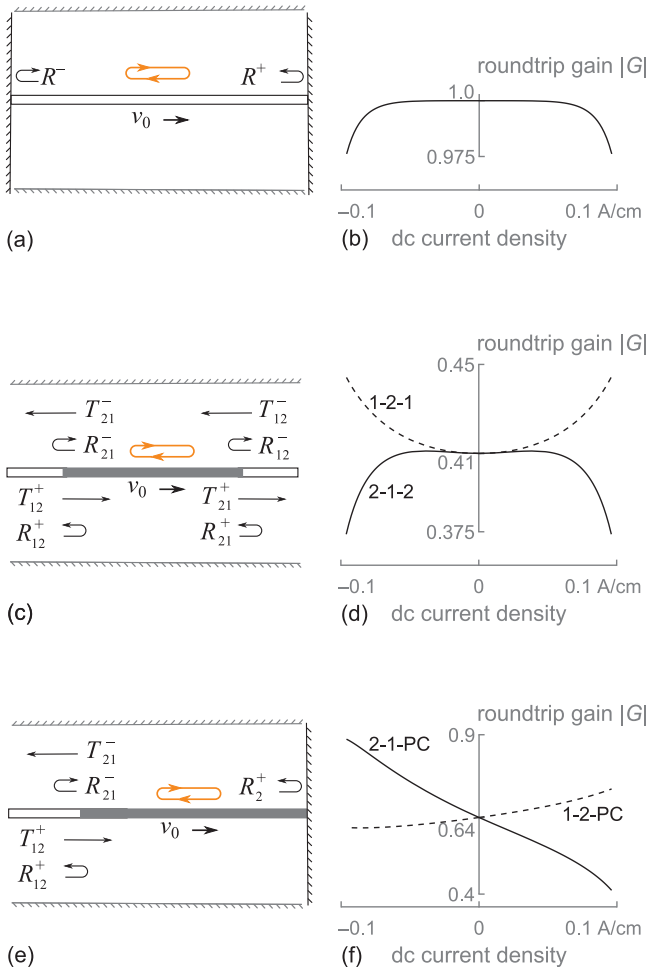

FIG. 8. Two-mirror resonators (a), (c), and (e), comprising the amplifying two-channel and conducting-plane interfaces. All of them have roundtrip gain (b), (d), and (f), smaller than unity. Here and in following figures, solid lines denote resonating sections with $n_1^{(0)} = 10^{11}\,\mathrm{cm}^{-2}$ while dashed lines denote sections with $n_2^{(0)} = 10^{12}\,\mathrm{cm}^{-2}$.

($10^{12}\,\mathrm{cm}^{-2}$) is sandwiched between channels with lower density ($10^{11}\,\mathrm{cm}^{-2}$), the roundtrip gain increases with drift, see the dashed line in Fig. 8(d). For the inverse density relationship, $|G|$ first slightly grows and then decays with the drift velocity. For both configurations, $|G|$ changes within 10% of its value without drift and remains far below the oscillation threshold.

Analogously, the relationship between the dc electron densities influences the properties of the resonator shown in Fig. 8(e). If the resonating section comprises the channel with the lower density, the roundtrip gain grows with negative and decays with positive drift velocities, see Fig. 8(f). The opposite occurs for the resonating section with the higher density. For the former configuration, the roundtrip gain is dominated by reflection from the conducting plane (see Fig. 6(a)), whereas for the latter one, this reflection coefficient differs little from unity (see Fig. 6(c)), and the roundtrip gain is determined mainly by the two-channel interface. The maximum roundtrip gain is about 0.9, still falling short of the oscillation threshold.

Closed at the right and open at the left, the configuration of Fig. 8(e) can be seen as a compound reflector for plasmons incident from the left. The total reflection coefficient is

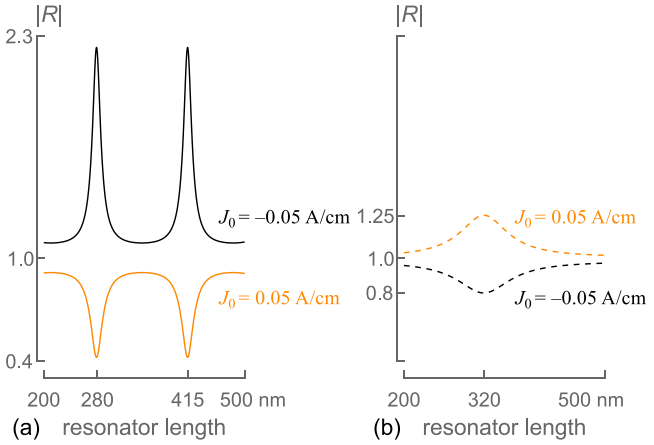

FIG. 9. The reflection coefficient of plasmon incident from the left on the composite mirror in Fig. 8(e) as a function of the length of the middle, resonating section. Its absolute value of can exceed that of individual interfaces, compare with Figs. 4 and 6.

$$R = R_{12}^{+} + \frac{T_{12}^{+}T_{21}^{-}R_{2}^{+}\mathrm{e}^{-\mathrm{j}(k_2^{+}-k_2^{-})l}}{1 - R_{21}^{-}R_{2}^{+}\mathrm{e}^{-\mathrm{j}(k_2^{+}-k_2^{-})l}}, \tag{36}$$

where l is the length of the resonating section. If the length is chosen properly, the total reflection coefficient can exceed that of the individual mirrors. For example, $|R|$ goes up to 2.3 for $J_0 = -0.05\,\mathrm{A/cm}$ if the middle section has the dc electron density of $10^{11}\,\mathrm{cm}^{-2}$, see Fig. 9(a). However, if the drift is in the opposite direction ($J_0 = 0.05\,\mathrm{A/cm}$), the reflection coefficient is less than unity. The situation reverses, in agreement with Fig. 8(f), if the resonating section has the dc electron density of $10^{12}\,\mathrm{cm}^{-2}$ the $|R| > 1$ if $J_0 > 0$, see Fig. 9(b), although the effect is less pronounced.

This compound mirror can be used to build more sophisticated resonators. Combining it with a conducting plane, we obtained the resonator of Fig. 10(a). It can be seen as comprising two coupled resonators, whose roundtrip gains can be found by multiplying the reflection coefficients of the form Eq. (36) by the reflection coefficient of one of the conducting planes. Assuming that the left resonator has the dc electron density of $10^{11}\,\mathrm{cm}^{-2}$, the right resonator the density of $10^{12}\,\mathrm{cm}^{-2}$ and comparing Figs. 6(a) and 9(b), we see that the absolute value of both reflection coefficients and, hence, of the roundtrip gain can exceed unity. The proper phase of G can be achieved by choosing the lengths of the sections. Assuming these are equal and range from 200 to 500 nm, Figs. 10(b) and 10(c) show the roundtrip gain for the two resonators on the complex plane. Both resonators can rise above the oscillation threshold (albeit at different lengths) when the drift velocity is directed to the right. For the opposite direction of drift, both resonators are below threshold. Although these results are not definitive, they clearly suggest advantageous properties of asymmetric configurations over symmetric ones: the former can allow oscillation to occur, while the latter apparently cannot. For field-effect transistors, analogous conclusions were reached by Dyakonov and Shur in Ref. 7. In contrast to their work, however, we consider structural asymmetry rather than asymmetry introduced by externally controlled boundary conditions.

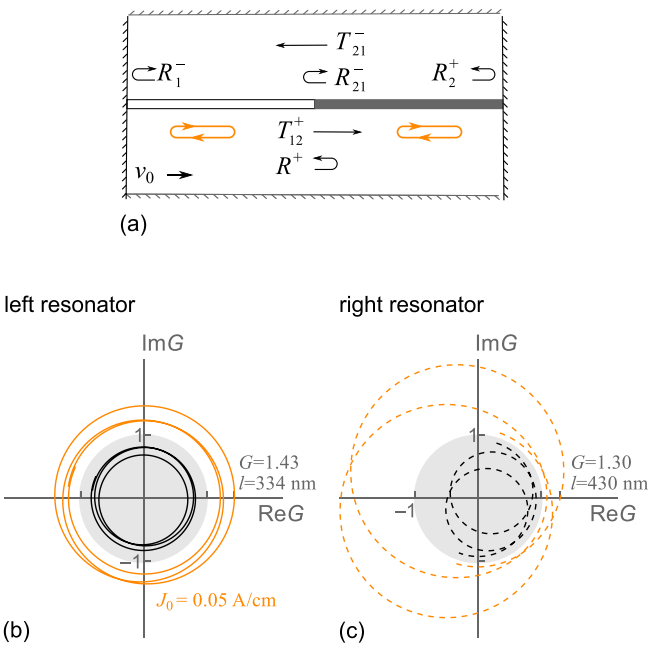

FIG. 10. Three-mirror oscillator comprising two different channels (a) and the complex roundtrip gain of the left (b) and right (c) resonators. The roundtrip gain can have real values exceeding unity.

V. CONCLUSIONS

As has been shown, drifting terahertz plasmons propagating along two-dimensional electron channels can be amplified by planar interfaces. Two such interfaces were discussed: one between a channel and a perfectly conducting plane and the other between two different channels. The conducting-plane interface has larger plasmonic reflection coefficients that exceed unity when the dc drift velocity points away from the plane. The results may have practical applications in amplification and generation of terahertz radiation. Particularly, Fabry-Perot resonators formed by the amplifying interfaces may have potential as terahertz oscillators. While the roundtrip gain of two-mirror resonators was below threshold, it rose above it for the three-mirror resonator.

Analyzing the interfaces, we were able to consider the whole mode spectrum—both plasmonic and non-plasmonic modes—by developing a mode-decomposition technique applicable in the presence of electron drift. In contrast to other approaches, this technique considers field distributions in the whole available space and uses rigorous electrodynamic boundary conditions. It is an excellent tool for design of plasmonic devices and its significance extends beyond the interfaces discussed here. In particular, it could be employed for the plasmonic configurations of recent experimental interest, such as field-effect transistors with continuous or periodic gate, source and drain contacts.

[1]Y.-S. Lee, *Principles of Terahertz Science and Technology* (Springer, New York, 2009).
[2]S. A. Mikhailov, Phys. Rev. B **58**, 1517 (1998).
[3]S. Riyopoulos, Phys. Plasmas **12**, 070704 (2005).
[4]S. M. Kukhtaruk, Semicond. Phys., Quantum Electron Optoelectron. **11**, 43 (2008).

[5]O. Sydoruk, V. Kalinin, and L. Solymar, Appl. Phys. Lett. **97**, 062107 (2010).
[6]V. Ryzhii, A. Satou, M. Ryzhii, T. Otsuji, and M. S. Shur, J. Phys.: Condens. Matter **20**, 384207 (2008).
[7]M. Dyakonov and M. Shur, Phys. Rev. Lett. **71**, 2465 (1993).
[8]F. J. Crowne, J. Appl. Phys. **82**, 1242 (1997).
[9]M. V. Cheremisin and G. G. Samsonidze, Semiconductors **33**, 578 (1999).
[10]F. J. Crowne, J. Appl. Phys. **87**, 8056 (2000).
[11]M. Dyakonov and M. Shur, Appl. Phys. Lett. **87**, 111501 (2005).
[12]O. Sydoruk, R. R. A. Syms, and L. Solymar, Appl. Phys. Lett. **97**, 263504 (2010).
[13]V. Ryzhii, A. Satou, and M. S. Shur, J. Appl. Phys. **93**, 10041 (2003).
[14]A. Satou, V. Ryzhii, and A. Chaplik, J. Appl. Phys. **98**, 034502 (2005).
[15]A. Satou, V. Ryzhii, V. Mitin, and N. Vagidov, Phys. Status Solidi B **264**, 2146 (2009).
[16]P. R. McIsaac, IEEE Trans. Microw. Theory Tech. **39**, 1808 (1991).
[17]G. I. Stegeman, A. A. Maradunin, and T. S. Rahman, Phys. Rev. B **23**, 2576 (1981).
[18]R. F. Oulton, D. F. P. Pile, Y. Liu, and X. Zhang, Phys. Rev. B **76**, 035408 (2007).
[19]S. E. Kocabas, G. Veronis, D. A. B. Miller, and S. Fan, Phys. Rev. B **79**, 035120 (2009).
[20]S. Thongrattanasiri, J. Elser, and V. A. Podolskiy, J. Opt. Soc. Am. B **26**, B102 (2009).
[21]A. L. Fetter, Ann. Phys. **81**, 367 (1973).
[22]S. J. Allen, D. C. Tsui, and R. A. Logan, Phys. Rev. Lett. **38**, 980 (1977).
[23]E. Batke, D. Heitmann, and C. W. Tu, Phys. Rev. B **34**, 6951 (1986).
[24]L. C. O. Súilleabháin, H. P. Hughes, A. C. Churchill, D. A. Ritchie, M. P. Grimshaw, and G. A. C. Jones, J. Appl. Phys. **76**, 1701 (1994).
[25]R. E. Tyson, R. J. Stuart, H. P. Hughes, J. E. F. Frost, D. A. Ritchie, G. A. C. Jones, and C. Shearwood, Int. J. Infrared Millim. Waves **14**, 1237 (1993).
[26]R. E. Collin, *Foundations for Microwave Engineering* (Wiley-IEEE, Hoboken, New Jersey, 2001).
[27]K. A. McIntosh, E. R. Brown, K. B. Nichols, O. B. McMahon, W. F. DiNatale, and T. M. Lyszczarz, Appl. Phys. Lett. **69**, 3632 (1996).
[28]W. W. Rigrod, J. Appl. Phys. **31**, 1147 (1960).
[29]O. Sydoruk, R. R. A. Syms, and L. Solymar, Opt. Express **20**, 19618 (2012).
[30]B. Sturman, E. Podivilov, and M. Gorkunov, Phys. Rev. B **76**, 125104 (2007).
[31]A. D. Bresler, G. H. Joshi, and N. Marcuvitz, J. Appl. Phys. **29**, 794 (1958).
[32]R. E. Collin, *Field Theory of Guided Waves* (Wiley-Interscience-IEEE, New York, 1991).